

IV.A.1h First-Principles Modeling of Hydrogen Storage in Metal Hydride Systems

J. Karl Johnson (Primary Contact) and David S. Sholl

University of Pittsburgh
1249 Benedum Hall
Pittsburgh, PA 15261
Phone: (412) 624-5644; Fax: (412) 624-9639
E-mail: karlj@pitt.edu

DOE Technology Development Manager:
Ned Stetson

Phone: (202) 586-9995; Fax: (202) 586-9811
E-mail: Ned.Stetson@ee.doe.gov

DOE Project Officer: Paul Bakke

Phone: (303) 275-4916; Fax: (303) 275-4753
E-mail: Paul.Bakke@go.doe.gov

Contract Number: DE-FC36-05GO15066

Subcontractor:

David S. Sholl, Georgia Institute of Technology,
Atlanta, GA

Project Start Date: March 1, 2005

Project End Date: February 28, 2010

- Specific energy: 1.5 kWh/kg
- Energy density: 0.9 kWh/L

Accomplishments

- Performed density functional theory (DFT) to predict the equilibrium crystal shape of seven metals and their hydrides via the Wulff construction.
- Computed the contribution to the thermodynamics of metal hydrides from surface energies of nanoparticles.
- Computed the change in temperature required to produce a pressure of H₂ of 1 bar upon desorption due to surface energies of nanoparticles.
- Calculated the structures and energetics of on the order of 100 different configurations of MgB₁₂H₁₂ and CaB₁₂H₁₂.
- Generated simulated X-ray diffraction patterns for these materials and performed a Boltzmann averaging of the structures.
- Generated energy histograms of energetics of MgB₁₂H₁₂ and CaB₁₂H₁₂.
- Investigated the energetics of poisoning of LiH, NaH, and KH surfaces by oxygen and water.
- Computed reaction pathways and energy barriers for H₂O dissociation on LiH, NaH, and KH surfaces.



Objectives

- Compute thermodynamics of metal hydride systems.
- Compute interfacial properties of hydrides.
- Address fundamental processes in hydrogenation.

Technical Barriers

This project addresses the following technical barriers from the Storage section (3.3.4) of the Hydrogen, Fuel Cells and Infrastructure Technologies Program Multi-Year Research, Development and Demonstration Plan:

- (A) System Weight and Volume
- (E) Charging/Discharging Rates (kinetics)
- (P) Lack of Understanding of Hydrogen Physisorption and Chemisorption

Technical Targets

This project is involved with developing new complex metal hydride materials that meet the DOE 2010 hydrogen storage targets:

Introduction

Complex metal hydrides such as alanates, amides and borohydrides of period 2 and 3 metals are promising materials for reaching high gravimetric and volumetric hydrogen densities for on-board fuel cell storage. A serious thermodynamic limitation of these materials is that high temperatures are often required to release H₂. The reaction free energy for decomposition of practical materials must lie in a narrow range of values to allow reversible hydrogenation and dehydrogenation at acceptable temperatures and pressures. In addition, the kinetics of hydrogenation and dehydrogenation must be acceptable.

Approach

We use quantum mechanical methods for computing the structural, electronic, energetic, and kinetic properties of complex hydrides and related materials. The specific method we use for most of our calculations

is periodic plane wave DFT, which is an approach for computing the approximate solution to the Schrödinger equation for condensed phase (solids) materials. This method requires as input at least an initial guess for the crystal structure of material to be modeled. The DFT method can then be used to optimize the atomic coordinates of each atom in the unit cell, the volume, and the shape of the unit cell. More importantly, we have developed a DFT-based method that can be used to quickly and reliably estimate the enthalpies of reaction for complex hydrides. We have used this method to screen over 300 possible hydrogen storage reactions and have identified several promising materials that have not previously been investigated. We can also calculate the free energies of reaction, including computing the entropic contributions through the phonon density of states. This is a much more computationally demanding approach – we have performed such calculations for a subset of the most promising reaction schemes identified from our screening calculations. We have also used DFT methods to compute kinetics for surface reactions as an initial approach for studying kinetics of reactions involving complex hydrides.

We have used the Vienna Ab initio Simulation Package (VASP) to perform most of the calculations in our work. We have used the gradient corrected approximation with the Perdew-Wang 91 functional. We have used both ultrasoft pseudopotentials and the projector augmented wave method.

Results

A useful way to characterize the thermodynamics of hydrogen release or uptake by metal hydrides is to determine the temperature at which the metal hydride is in equilibrium with the metal when the H₂ pressure is 1 bar [1]. Under these conditions the free energy, or equivalently, the grand potential, of the two systems are equal [2]. For bulk samples, the grand potential can be estimated using DFT calculations by

$$\Omega(T) = E - \frac{1}{2} (E_{H_2} + E_{ZPE,H_2} + \tilde{\mu}_{H_2}) n^H \quad (1)$$

where E is the total energy for the solid of interest computed from DFT, the quantities inside the parentheses are the energy, zero point energy (ZPE), and chemical potential of molecular H₂, and n^H is the number of H atoms per metal atom in the solid [3-5]. This expression neglects ZPE in the solid and temperature dependent vibrational contributions to the solid's free energy; we return to these approximations below. From this expression for the grand potential, it follows that the bulk metal hydride and metal are in equilibrium when

$$\tilde{\mu}_{H_2}(T, P_{H_2} = 1 \text{ bar}) = \beta = \frac{2}{n^H} (E_{MH}^{bulk} - E_M^{bulk}) - (E_{H_2} + E_{ZPE,H_2}) \quad (2)$$

Here, MH and M denote the metal hydride and metal, respectively. To extend this expression to solid particles of finite size, the influence of surface energy on the overall energy of the solids must be included. Using quantities accessible via DFT calculations based on slab geometries, the surface energy is

$$\gamma = [E^{slab} - NE^{bulk}] / A \quad (3)$$

where E^{slab} is the total energy of the slab containing N metal atoms, E^{bulk} is the total energy of the bulk material per metal atom, and A is the total surface area exposed by both sides of the slab [6-8]. Here, the slab energy is defined using a slab that has been geometry optimized to include the effects of surface relaxation. Nanoparticles of a metal and its metal hydride are in equilibrium when

$$\tilde{\mu}_{H_2}(T, P_{H_2} = 1 \text{ bar}) = \beta + \alpha / N, \quad (4)$$

where

$$\alpha = \frac{2}{n^H} \left(\sum_i (A_{MH,i}^{surf} \gamma_{MH,i}^{surf}) - \sum_j (A_{M,j}^{surf} \gamma_{M,j}^{surf}) \right) = \frac{2}{n^H} \Delta(A^{surf} \gamma^{surf}) \quad (5)$$

The summations are necessary here to allow for particles that expose multiple surfaces. Once $\tilde{\mu}_{H_2}(T, P_{H_2})$ is known from either Eq. (2) or (5), the temperature at which the metal and metal hydride are in equilibrium, T_{eq} , is defined. In calculating T_{eq} , we assume that H₂ is an ideal gas.

An alternative way to describe the thermodynamic effects of nanosizing is to use the change in enthalpy between the reaction involving a nanoparticle and the reaction for the bulk materials,

$$\Delta\Delta H = \Delta H(N) - \Delta H(\infty) \quad (6)$$

In terms of the quantities defined above, this enthalpy change is simply

$$\Delta\Delta H = -\frac{\alpha}{N} \quad (7)$$

To make use of the formalism above, we need to determine the areas and surface energies of the surfaces exposed by each nanoparticle of interest. If the surface energies of each possible surface are known, the Wulff construction can be used to predict the equilibrium crystal shape (ECS) of the material [6,7,9]. To apply the Wulff construction, we used DFT to calculate the surface energy of each low index surface of seven elemental metals and their hydrides, as summarized in Table 1. A convenient feature of these low index surfaces for all the hydrides we considered is that each layer normal to the surface has the same stoichiometry as the bulk hydride. This means that there is no ambiguity in defining the termination of these surfaces [10].

Using the surface energies calculated from DFT, we applied the Wulff construction for the seven metals and metal hydrides we considered. We examined five low

index surfaces for Sc, and all of these surfaces appear on the ECS, with the (10 $\bar{1}$ 1) and (10 $\bar{2}$ 1) surfaces defining about 70% of the entire surface area. The (10 $\bar{2}$ 0) surface is predicted to only account for 0.4% of the particle's total surface area. The same set of five surfaces was considered for Ti. For Ti, only four surfaces feature on the ECS, and the (10 $\bar{2}$ 1) surfaces defines about half of the total surface area. Our calculated surface energies for Ti differ in several respects from the values reported by Wang, Zhang, and Xu using calculations with the modified embedded atom method (MEAM) [11]. For example, our calculations indicate that the (10 $\bar{2}$ 1) surface has the lowest surface energy, while Wang et al.'s calculations suggested that the (10 $\bar{2}$ 0) surface has a lower surface energy than (10 $\bar{2}$ 1). Although DFT calculations do not give exact results for surface energies, it seems likely that our DFT results are more reliable than results from the semi-empirical MEAM. The ECS of ScH₂ and TiH₂ are much simpler than their metal counterparts, an observation that can be understood by noting that the partially ionic nature of these materials makes their surface energies much more anisotropic than the surface energies of elemental metals. These hydrides have only (111) surfaces on their ECS. The contribution of each surface to the total surface area on the ECS of each of the seven metals and hydrides we have considered is summarized in Table 1.

From the calculated surface energies and ECS, we used Eq. (5) to describe the influence on particle size on the thermodynamics of hydrogen evolution. Our results are summarized in Figure 1, which shows the difference between the equilibrium temperature, T_{eq} , for

a nanoparticle and a bulk material. In this figure, the size of the metallic nanoparticle is shown by converting the volume of the nanoparticle with the predicted Wulff ECS to a spherical particle with the same bulk density. The numerical values of α for each metal/metal hydride pair are defined in Table 2 by listing $\alpha N^{-2/3}$, a quantity that is independent of N . An initial observation from Figure 1 and Table 2 is that both positive and negative deviations of the transition temperature with respect to the bulk material exist. For MgH₂/Mg and NaH/Na, the sign of α is positive, so the transition temperature decreases as the particle size is reduced. The opposite trend is seen for the other five metal/metal hydride pairs.

A second observation from Figure 1 is that the changes in the transition temperature relative to the bulk materials are, on the whole, small. For metal particles with radius 10 nm, the effects from the exposed surfaces change the transition temperature by less than 20 K for every material. For the two cases where the transition temperature is lower for nanoparticles than for the bulk material, the temperature is only reduced by 33 (16) K for MgH₂/Mg (NaH/Na) for the extreme case of a nanoparticle having a radius of 1 nm. The largest effect of nanoparticle size is predicted for VH₂/V. If we consider a V nanoparticle with radius 5 nm as an example, the transition temperature in this case is only 30 K larger than for the bulk system. We note that for most systems it is desirable to reduce the transition temperature or heat of reaction. However, for AlH₃, it would be useful to increase the transition temperature (or equivalently, the heat of reaction) because at equilibrium, AlH₃ decomposes at temperatures that are

TABLE 1. Summary of the surfaces examined for each material in applying the Wulff construction to form the ECS. The final column indicates the fraction of the total surface area on the ECS associated with each surface.

Space group	Material(s)	Surfaces examined	Surfaces on ECS
Im $\bar{3}m$	V	(111), (110), (100)	(110) – 70%, (100) – 24%, (111) – 6%
	Li	(111), (110), (100)	(110) – 53%, (100) – 39.3%, (111) – 7.7%
	Na	(111), (110), (100)	(110) – 78.1%, (100) – 21.2%, (111) – 0.7%
P6 ₃ /mmc	Sc	(0001), (10 $\bar{1}$ 0), (10 $\bar{1}$ 1), (11 $\bar{2}$ 0), (11 $\bar{2}$ 1)	(10 $\bar{1}$ 1) – 38.7%, (11 $\bar{2}$ 1) – 33%, (0001) – 15.8%, (10 $\bar{1}$ 0) – 12.1%, (11 $\bar{2}$ 0) – 0.4%
	Ti	(0001), (10 $\bar{1}$ 0), (10 $\bar{1}$ 1), (11 $\bar{2}$ 0), (11 $\bar{2}$ 1)	(11 $\bar{2}$ 1) – 55.5%, (10 $\bar{1}$ 1) – 24.5%, (0001) – 17.2%, (10 $\bar{1}$ 0) – 2.8%
	Mg	(0001), (10 $\bar{1}$ 0), (10 $\bar{1}$ 1), (11 $\bar{2}$ 0), (11 $\bar{2}$ 1)	(10 $\bar{1}$ 1) – 38%, (10 $\bar{1}$ 0) – 37.8%, (0001) – 24.2%
Fm $\bar{3}m$	Al	(111), (110), (100)	(111) – 75.5%, (100) – 24.5%
Fm $\bar{3}m$	VH ₂	(111), (110), (100)	(111) – 100%
	LiH	(111), (110), (100)	(100) – 100%

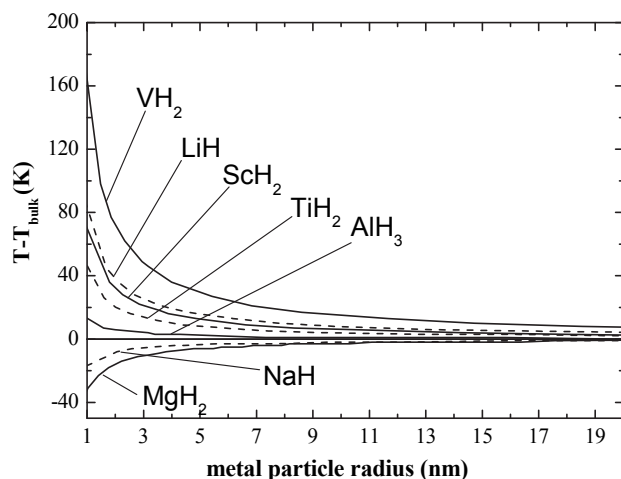


FIGURE 1. The variation in the metal/metal hydride transition temperature relative to the result for a bulk material determined as described in the text.

too low for practical applications [12]. The nanoparticle transition temperature does indeed increase for the AlH_3/Al system, as seen in Figure 1, but the effect is extremely small, increasing T_{eq} by only 13 K for the extreme case of a metal nanoparticle 1 nm in radius.

Our results are shown in Figure 2 in terms of the enthalpy instead of temperature. As has already been discussed by focusing on the transition temperatures for these materials, the enthalpy changes associated with even very small nanoparticles are small.

To consider the physical source of the trends in α listed in Table 2, we calculated the charge associated with the H atoms in each metal hydride we examined using a Bader charge decomposition [13]. The resulting charges are shown in Figure 3. With the exception of LiH, there is a distinct correlation between α and the H atom Bader charge in the hydride, with the most (least) ionic materials being associated with positive (negative) values of α .

TABLE 2. The numerical coefficient, α , that controls nanoparticle thermodynamic effects for the seven systems we have considered, where N is the number of metal atoms in the nanoparticle.

System	$\alpha/N^{2/3}$ (eV)
VH_2/V	-1.608
LiH/Li	-0.822
ScH_2/Sc	-0.667
TiH_2/Ti	-0.461
AlH_3/Al	-0.107
NaH/Na	0.134
MgH_2/Mg	0.296

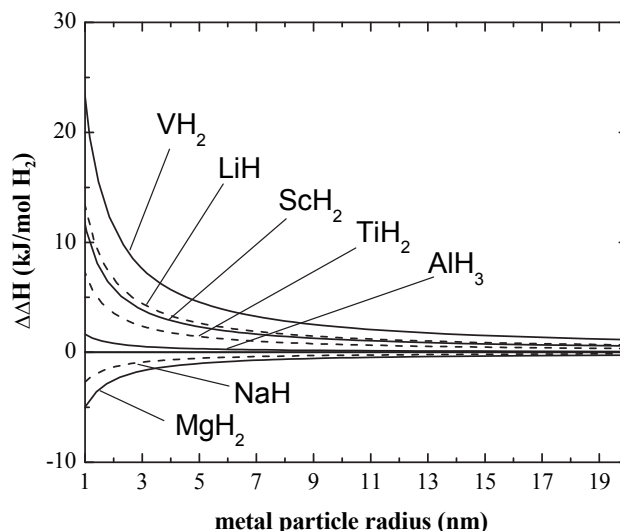


FIGURE 2. The variation in the metal/metal hydride reaction enthalpy relative to the result for a bulk material determined as described in the text.

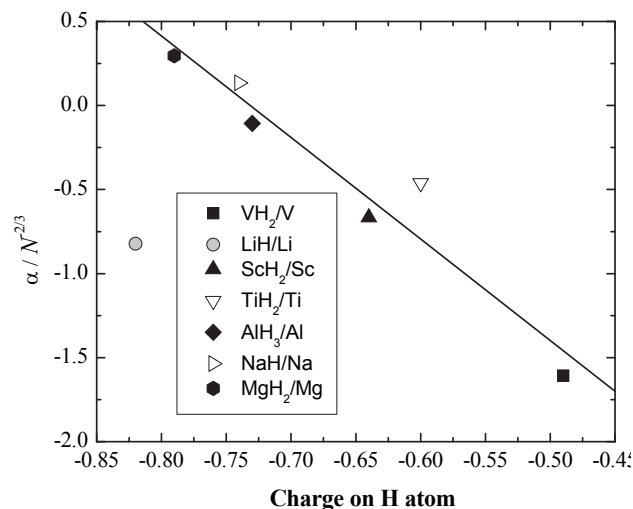


FIGURE 3. Plot of $\alpha/N^{2/3}$ as a function of the charge on the H atom in the bulk hydride as computed by Bader charge analysis, where α is the parameter that controls nanoparticle thermodynamic effects and N is the number of metal atoms in the nanoparticle. The line is a linear fit to all systems except LiH/Li.

Conclusions and Future Directions

- We have computed the effects of nanoparticle surface energies on the thermodynamics of hydride reactions. We have found that for the simple hydrides we tested that the effect of nanosizing is to increase the temperature required to generate one bar of H_2 pressure, which is just the opposite of the effect desired in most cases. Moreover, the change in temperature is typically very small.

- Our calculations on nanoparticles cannot explain the experimental results for complex hydrides confined in porous materials.
- We have studied the kinetics and of poisoning of metal hydride surfaces in an effort to explain the observed differences in reversibility for reactions involving $MH+Al$, for $M=Li, Na,$ and K . We found that all three hydrides were readily poisoned by water and oxygen. However, poisoning of LiH by O was seen to form a surface $LiOH$ structure that is commensurate with the LiH lattice and very similar to the $LiOH$ bulk structure.
- We plan to finish up calculations of multiple step reactions and metastable reactions.
- We will publish a paper on the effects of amorphous closo-borane materials on the reversibility of borohydride compounds.

FY 2009 Publications/Presentations

1. Ki Chul Kim, Bing Dai, J. Karl Johnson and David S. Sholl, "Assessing nanoparticle size effects on metal hydride thermodynamics using the Wulff construction", *Nanotechnology*, **20**, 204001 (2009).
2. Bing Dai, Rees B. Rankin, J. Karl Johnson, Mark D. Allendorf, David S. Sholl, Nikolai A. Zarkevich and Duane D. Johnson, "Influence of Surface Reactions on Complex Hydride Reversibility", *Journal of Physical Chemistry C*, **112**, 18270–18279 (2008).
3. J. Karl Johnson, "Quantum and Statistical Mechanical Modeling of Adsorption, Transport, and Reactions at Surfaces", *Dynamics and Chemistry of Surfaces and Interface Basic Research Workshop* June 23–25, 2009, 700 Drayton Streetm, Savannah, GA, USA.
4. J. Karl Johnson, "Adsorption and diffusion of hydrogen in nanoporous materials", 237th ACS National Meeting, March 22–26, 2009 in Salt Lake City, Utah.
5. J. Karl Johnson, "Atomistic Modeling of Hydrogen Storage in Complex Metal Hydrides", University of Nebraska-Lincoln, Department of Chemistry Colloquium, February 13, 2009, Lincoln, NE.
6. J. Karl Johnson, "Hydrogen Storage: Insights from Atomistic Modeling", Rutgers University, Department of Chemical & Biochemical Engineering, Departmental Seminar Series, February 11, 2009, Piscataway, NJ.
7. J. Karl Johnson, Ki-Chul Kim, Anant Kulkarni, and David S. Sholl, "Predicting Metal Hydride Reactions from First Principles", *AIChE Annual Meeting*, Philadelphia, PA, November 16–24, 2008.
8. Anant D. Kulkarni Lin-Lin Wang, Duane D. Johnson, David S. Sholl, and J. Karl Johnson, "First Principles Study of Dehydrogenation Reaction Intermediates of Complex Metal Borohydrides," *PA-OH-WV Simulators Meeting, Pittsburgh*, PA 9 June 2009.

References

1. Züttel, A. *Mater. Today* **2003**, *6*, 24.
2. Akbarzadeh, A.; Ozolinš, V.; Wolverson, C. *Adv. Mat.* **2007**, *19*, 3233.
3. Raybaud, P.; Hafner, J.; Kresse, G.; Kasztelan, S.; Toulhoat, H. *J. Catal.* **2000**, *189*, 129-146.
4. Alapati, S.V.; Johnson, J.K.; Sholl, D.S. *J. Phys. Chem. C* **2007**, *111*, 1584-1591.
5. Stampfl, C. *Catal. Today* **2005**, *105*, 17-35.
6. Shi, H.Q.; Stampfl, C. *Phys. Rev. B* **2008**, *77*, 094127.
7. Soon, A.; Wong, L.; Delley, B.; Stampfl, C. *Phys. Rev. B* **2008**, *77*, 125423.
8. Rankin, R.B.; Sholl, D.S. *J. Chem. Phys.* **2006**, *124*, 074703.
9. Wulff, G.Z. *Krist. Mineral.* **1901**, *34*, 449-530.
10. Asthagiri, A.; Sholl, D.S. *J. Chem. Phys.* **2002**, *116*, 9914-9925.
11. Wang, D.-D.; Zhang, J.-M.; Xu, K.-W. *Surf. Sci.* **2006**, *600*, 2990-2996.
12. Graetz, J.; Reilly, J.J.; Kulleck, J.G.; Bowman, R.C. *J. Alloys Compd.* **2007**, *446*, 271-275.
13. Henkelman, G.; Arnaldsson, A.; Jonsson, H. *Comp. Mat. Sci.* **2006**, *36*, 354-360.